Available online at www.sciencedirect.com
ScienceDirect
Engineering Structures 30 (2008) 909–929
ENGINEERING STRUCTURES
www.elsevier.com/locate/engstruct

Multiple crack identification of a free–free beam with uniform material property variation and varied noised frequency

Ren-Jeng Lin[a,*], Fu-Ping Cheng[b,1]

[a] *Department of Civil Engineering, National Chiao Tung University, P.O. Box 61, Lung-Tan, Taoyuan 32599, Taiwan, ROC*
[b] *Department of Civil Engineering, National Chiao Tung University, Hsin-Chu 300, Taiwan, ROC*

Received 28 June 2006; received in revised form 26 November 2006; accepted 18 March 2007
Available online 23 July 2007

Abstract

It is common to apply damage-sensitive features from vibration responses of a structure to assess structural damage. Few damage identification algorithms have focused on the material variation and measurement noise. For engineering practices, the material variation could be caused by many reasons and there always exists a certain level noise in measurement; those facts may affect the features that are used for structure monitoring and also lead to inaccurate assessment.

In this research the authors have proposed a model to assess the statistical structural damage of a beam structure. The modal curvature-base feature was used to identify crack locations. The statistical damage databases were built by applying the Latin hypercube sampling method in Monte Carlo simulation. By mapping features of noised modal frequency to the statistical damage database, the damage probabilities among various crack depths were estimated; the statistical significance of damage level was examined by the t-test. Simulated beams and their experimental modal analysis data demonstrated the assessment procedures. The authors concluded that the proposed algorithm was robust and able to identify the damage of a free–free beam with uniform mass density and stiffness variations incorporated with noise in measured frequency.

Keywords: Multiple cracks; Identification; Damage assessment; Beam; Variation; Monte Carlo

1. Introduction

Structure health monitoring has been receiving increasing interest in both academic research and industry applications for several decades [3]. An extensive literature review for 1975–1996 by Doebling et al. [5] was made at the Los Alamos National Laboratory (LANL). The review focused on methods and data required for detecting, locating, and characterizing structure damage by examining the changes in various types of measured structure responses. The report also summarized the state of the art of structural health monitoring technology and the applications of various damage identification methods for different types of structure. But almost none of the several hundred cited references took any statistical approach to access the damaged systems [18]. Another comprehensive updated literature review for 1996–2001 by Sohn et al. was also published by LANL [18]. The authors of the updated report mentioned that due to the observations of environment variability and operational conditions for long-term monitoring, the authors believe that structure health monitoring is fundamentally a statistical pattern recognition problem.

Sikorsky et al. [16] reported that there were 3.8% and 3.2% variations in first and second modal frequencies under 40 °C temperature variation over a 24 month observation for a bridge in Coachella Valley, California. Ko et al. [10] also recorded 12 month data from the cable stayed Ting-Kau bridge in Hong Kong and concluded that a 2.01%–16.67% modal frequency change occurred for the first 11 modes on about 50 °C temperature variation, and also that the frequencies were decreased with increased temperature. Xia et al. [21] had constructed a reinforced concrete slab to investigate the correlations between vibration parameters and environment

* Corresponding author. Tel.: +886 912 886036; fax: +886 3 4993036.
E-mail addresses: renjeng.lin@msa.hinet.net, simtech.tw@hotmail.com (R.-J. Lin), fpcheng@mail.nctu.edu.tw (F.-P. Cheng).
[1] Tel.: +886 3 5712121x54919; fax: +886 3 5718129.

0141-0296/$ - see front matter © 2007 Elsevier Ltd. All rights reserved.
doi:10.1016/j.engstruct.2007.03.017

conditions. Data collected over 24 months showed there were 30 °C temperature and 65% humidity changes, and the frequencies had about 3%–10% variations. The results also show that the frequencies decreased and damping ratio increased with the increased temperature and humidity. Other research also showed the same conclusion that the frequencies decreased as temperatures increased [4,14,17].

When the environmental variability or operating conditions are an important issue, they will affect the damage-sensitive features and may mask out real damage state and lead to inaccurate assessment. Xia et al. [21] advised that the vibration properties should be corrected to the same environmental conditions for structures in undamaged and damaged states. The same suggestion by Sohn et al. [18] was to carry out the data normalization so that the signal changes caused by variations can be separated from structural changes. Doebling and Farrar [6] are pioneers in examining the statistical significance of damage identification results using data collected on the I-40 highway bridge. Xia and Hao [20] assumed the prior model and measure data fit for the Gaussian distribution and proposed a two-stage statistical identification algorithm. By taking the statistical operation of a second-order Taylor's expansion on the model updating equation, the authors estimated the probability of damage existence by comparing the statistical distribution of element stiffness between undamaged and damaged states. Furukawa and Otsuka [9] removed the Gaussian distribution assumption on variability and measurement noise, and then identified the possible damage of elements by the frequency response function changes from the intact state deterministically. Then, they adopted the hypothesis test based on the bootstrap resampling technique [7] to exclude the undamaged elements from the damaged element candidates. By the iterative zoom-in process, satisfactory results will be obtained within 3 iterations for a large simulated system with 10% noise.

A closed-form derivation of a statistical damage identification algorithm has many good aspects. However, for a complex system there may be difficulties, one example being to derive the distribution types of element stiffness for significant verification [20]. Instead, the fast development of computer hardware has made the use of computation intensive algorithms possible. Due to the uncertainty of related analysis of complex systems, the Monte Carlo technique [15] was the simplest and most widely employed method. With the modification to Monte Carlo techniques, the Latin hypercube sampling (LHS) [11,19] provided an efficient way of sampling variables with distributions by assuming that all the variables are independent of each other. Although the efficiency differed in various applications, some research reported that it saved more than 50% of computer effort [12]. Besides, compared to rederivation of a rigorous statistical damage identification algorithm, there is less effort spent and it is more intuitive to incorporate the well-developed deterministic damage identification algorithm with a Monte Carlo based simulation technique.

In this research, the authors have assumed that the environmental variability caused the stiffness and mass variation on the entire beam uniformly, and noise in the measured frequency was assumed. The authors build up the statistical damage reference database that was incorporated with various property variations and damage states by applying the LHS techniques. Then, they assess the statistical significance by applying the vibration features of an unknown damaged state and the t-test [8] to identify its damage locations. At last, the damage probability among the possible severity was estimated by mapping the vibration features to the statistical damage database. Demonstration examples showed that the approach was able to identify the damage of a beam structure with uniform mass and stiffness variations and incorporated with noise polluted measured frequency.

2. Simulated beam model and experimental modal analysis (EMA)

An accurate prior model is essential for the supervised damage assessment algorithm [18]. The following sections focus on the correctness of simulated model when compared to the EMA of real sample beams. The error or uncertainty of the finite element prior model can be included in the statistical model by assigning the variances of stiffness and mass directly.

2.1. Simulation of cracked beam

Cracked beam modeling will deal with the cracked zone and the intact zone. Thick shell elements [22] were used for the intact zone. For the cracked zone, the authors applied thick shell elements combined with a degenerated quarter point singularity formulation [2]. The simulation results are accurate in frequencies and mode shapes among sample beams. The mean error of modal frequencies was under 0.3% and the maximum error was under 0.8% for the lowest three modes. The modal assurance criterion (MAC) [1] was used to measure the accuracy of mode shapes between analytical and experimental models. When the MAC is close to 1.0, the results have a good correlation, and they are uncorrelated when the MAC is close to 0.0. By combining the calculations of different mode shapes of analytical and experimental data, we can construct the MAC in matrix form. From the calculation, we found that the diagonal terms in MAC matrix were all larger than 0.997, and the off-diagonal terms were all under 0.064 for the lowest three modes for all sample beams.

2.2. Configurations of cracked beam samples

The sample beams are all rectangular-sectioned mild steel bar, 600 mm (L) × 16 mm (W) × 16 mm (H) in size and divided into two categories. The first group was for intact beams, named S. The other group was for damaged beams, named from A to N. All the damaged beams were manufactured with a high-accuracy wire-cut to produce an artificial slot with a specific crack location and depth. Beam-M was a multiple-crack beam; all other beams were single-crack beams. The configuration of the sample beams can be found in Table 1.

Table 1
Configurations of sample beams

Sample no.	Sample name	1st crack (location, depth) (in mm)	2nd crack (location, depth) (in mm)
1	A	(131.0, 6.0)	None
2	B	(131.0, 8.0)	None
3	C	(131.0, 10.0)	None
4	D	(187.0, 6.0)	None
5	E	(187.0, 8.0)	None
6	F	(187.0, 10.0)	None
7	N	(243.0, 3.0)	None
8	G	(243.0, 6.0)	None
9	H	(243.0, 8.0)	None
10	I	(243.0, 10.0)	None
11	J	(300.0, 6.0)	None
12	K	(300.0, 8.0)	None
13	L	(300.0, 10.0)	None
14	M	(131.0, 8.0)	(243.0, 10.0)
15	S	Intact beam (without damage)	

2.3. Experimental modal analysis of cracked beam

A PC-based data acquisition system was used for modal test experiments. The system consists of a PC, an AD/DA module, accelerometers, a hammer, and power amplifiers. The sampling rate was 2000 Hz, with 1.25 Hz resolution, with a fixed sensor at ends of sample beam; 12–18 locations were selected for hammer impact, and each location takes 15 impacts on average. For the simulation of the free–free boundary condition, two rubber strings was used to suspend the sample beams. After the modal data were collected, STAR® modal analysis software was used for modal analysis to identify the modal parameters. We should recall that for practical engineering the "fixed response" method of EMA should change to "fixed impact" to save the labor work.

3. Dynamic characteristics of cracked beam with related to damage location and its extents

A beam with a crack will reduce its stiffness when compared with a beam in the intact state. Its frequencies will be reduced; the mode shapes and curvature mode shapes will be changed, too. When the system mass density or Young's modulus of the entirely structure is varied for certain reason, its frequencies will change too, but there will be no effect on the mode shapes and curvature mode shapes. By selecting appropriate features from vibration responses, we can detect the damage location and identify its severity. The simulation and experimental results shown in the following sections supported these conclusions.

3.1. Definition of the LDI

The previous researchers Pandey et al. [13] introduced the application of curvature mode shape for the detection of damage location. In the research, the authors defined another index for crack location detection, named the LDI (Location Detect Index). For an Euler–Bernoulli beam, the strain energy (U_i) of an intact beam with respect to mode shape i (ϕ_i) can be expressed as

$$U_i = \frac{1}{2}\int_0^l EI\left(\frac{\partial^2\phi_i(x)}{\partial x^2}\right)\mathrm{d}x \tag{1}$$

where EI, l are the section rigidity and the length of beam. For an infinitesimal length $\mathrm{d}x$ located at x_j along the beam's axis, the strain energy of length $\mathrm{d}x$ can be expressed by u_{ij},

$$u_{ij} = \frac{1}{2}EI(x_j)\left(\frac{\partial^2\phi_i(x_j)}{\partial x^2}\right)^2\mathrm{d}x. \tag{2}$$

The authors define the energy fraction with respect to total energy of entire beam U_i as F_{ij},

$$F_{ij} = u_{ij}/U_i \tag{3}$$

$$\int_0^l F_{ij} = 1.0. \tag{4}$$

For the same operation, for a cracked beam, we have

$$U_i^* = \frac{1}{2}\int_0^l EI\left(\frac{\partial^2\phi_i^*(x)}{\partial x^2}\right)^2\mathrm{d}x \tag{5}$$

$$u_{ij}^* = \frac{1}{2}EI(x_j)\left(\frac{\partial^2\phi_i^*(x_j)}{\partial x^2}\right)\mathrm{d}x \tag{6}$$

$$F_{ij}^* = u_{ij}^*/U_i^* \tag{7}$$

$$\int_0^l F_{ij}^* = 1.0 \tag{8}$$

where U_i^*, u_{ij}^*, ϕ_i^*, and F_{ij}^* are strain energy, strain energy of infinitesimal length $\mathrm{d}x$, mode shape i and energy fraction of cracked beam, respectively.

Let $\delta\kappa_{ij}$ be the temporary feature for location detection; it can be expressed as follows:

$$\delta\kappa_{ij} = F_{ij}^* - F_{ij}. \tag{9}$$

By the normalization operation, we have the location's discrimination feature LDI as follows:

$$\mathrm{LDI}(x_j) = \delta\kappa_{ij} \Big/ \left\{\frac{1}{2} EI(x_j)\right\} = \left(\frac{\partial^2 \phi_i^*(x_j)}{\partial x^2}\right)^2 \Big/ U_i^* - \left(\frac{\partial^2 \phi_i(x_j)}{\partial x^2}\right)^2 \Big/ U_i. \quad (10)$$

When we plot the LDI along beam axis, we will have the curve of the LDI curve.

By reviewing the simulation results, we found that a sharp peak indicated the location of cracks. The deeper crack depth made the peak of the LDI curve sharper. From the experimental modal analysis (EMA) results we also found that the sharp peaks were located closed to the crack location for different modes and the deeper crack depths made the peak sharper for LDI curves. The LDI works well on both the simulation and experimental modal analysis data.

3.2. Definition of FCI curve

The authors define the frequency change as a specific point on the FCI (Frequency Change Index) curve. It can be expressed as

$$\mathrm{FCI}(\Delta f_{i,\mathrm{damaged}}) = \frac{f_{j,\mathrm{intact}} - f_{j,\mathrm{damaged}}}{f_{j,\mathrm{intact}}} * 100\,(\%) \quad (11)$$

where $f_{j,\mathrm{intact}}$ and $f_{j,\mathrm{damaged}}$ are the frequency of mode j for the intact and damaged beam respectively. Each FCI curve was made by a frequency change due to a constant crack depth moving along the beam axis. The specific point on each FCI curve represents a damage state (certain crack depth and location) of the cracked beam. We observed that the deeper crack depth made the larger amplitude on the FCI curve, and if the damage is located at the node of the curvature mode shape, there will be no frequency changes in the FCI. We have also found that the simulation results were consistent with the EMA.

3.3. FCI for depth identification of single-crack beam for a property-invariant system with noise-free measurement

When we have the noise-free measured frequency from the EMA for a property-invariant structure system, the table lookup process was adopted for damage severity estimation. From the schematic figures illustrated in Fig. 1, after the crack location is identified by the LDI, we can identify the unknown crack depth by applying linear interpolation between two FCI curves. These FCI curves were above and below the EMA's on the specific crack location from the simulation database. The linear interpolation for unknown crack depth (β_x) is shown below, and is illustrated in Fig. 2.

$$\beta_x = \beta_l + \frac{\Delta f_x - \Delta f_l}{\Delta f_u - \Delta f_l} * (\beta_u - \beta_l) \quad (12)$$

where Δf_x was calculated by Eq. (11) from the EMA measured frequencies (f_x) for an unknown damage state, Δf_u and Δf_l were points on FCI curves that were also calculated by Eq. (11) on the above frequency (f_u) and below frequency (f_l) compared with the EMA measured frequencies (f_x), and β_u and β_l were crack depths with respect to Δf_u and Δf_l respectively. By inserting Eq. (11) into Eq. (12), we obtain Eq. (13) as follows:

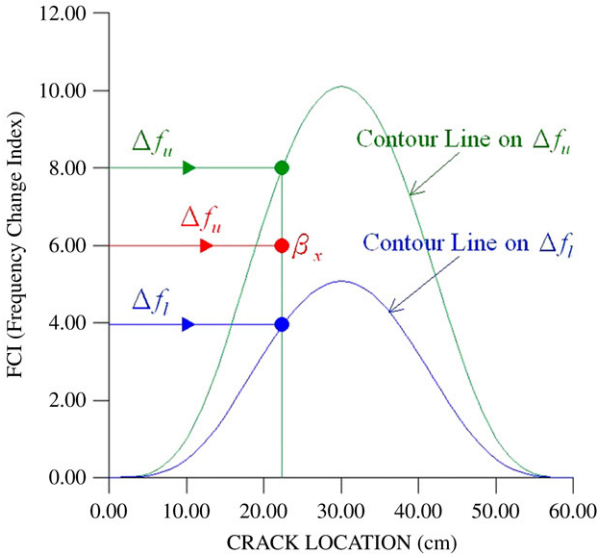

Fig. 1. Crack depth assessment for property invariant beam structure.

$$\beta_x = \beta_l + \frac{f_x - f_l}{f_u - f_l} * (\beta_u - \beta_l). \quad (13)$$

3.4. FCI for depth identification of multiple-crack beam for a property-invariant system with noise-free measurement

The LDI curve can be applied to the multiple cracks case directly. However, the authors should do a little modification for depth identification of multiple cracks case due to the frequencies change were affected by all the cracks in the beam. A 2-crack beam is discussed for demonstration.

Once we have the crack locations from the LDI curve, we should build up an FCI database of varied depths based on these known locations. On comparing the noise-free frequencies from EMA with the frequencies of an intact beam from simulation, the FCI curves among different modes on the specific cracked configuration can be obtained. We can plot the contour lines of frequency change on each mode as shown in Fig. 3. Then the crack depths were identified by the intersection of two FCI contour lines as shown in Fig. 4. We should notice that when the number of cracks is larger than two, with the same FCI database, we could always apply a suitable mathematical tool to determine all the depths simultaneously.

3.5. Stiffness and mass density variant effects on LDI and FCI

In order to clarify the effect of material property variation on the LDI and FCI, the authors prepared a simulated cracked beam (Beam-I, crack located 243 mm, depth 10 mm) with a series combinations of different levels of mass density and

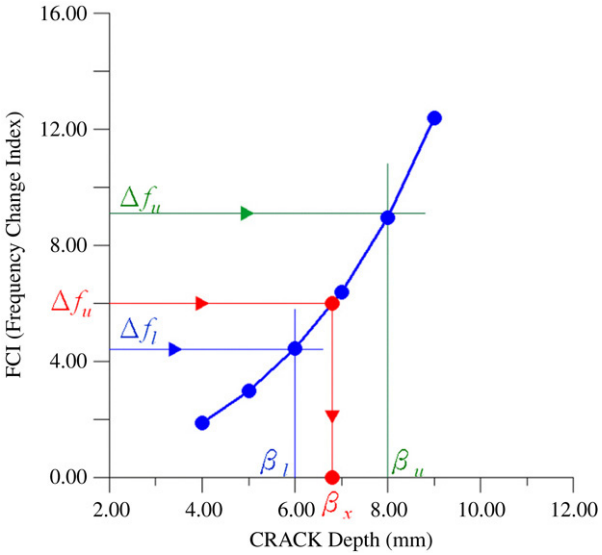

Fig. 2. Crack depth assessment for property invariant beam structure.

Young's modulus variance that ranged from ±80% to ±120% of their mean value.

Due to the stiffness and mass variation affecting the structure in a uniform way along the entire beam structure, the mode shape changed insignificantly on the variations, and the algorithm for crack location identification was held for the property variant systems. From the observation, we found that the LDI indicated the crack location clearly among various variation scenarios. The LDI works well and is robust for systems with uniform material property variations. Then, by reviewing the results again, we found that the FCI changed approximately ±20% when compared to the no variant system. Hence, we should take into account the influences of property variations when applying the FCI for severity assessment. In the research, the authors represent these effects by statistical FCI databases, which were generated by LHS sampling in Monte Carlo simulation on a beam with certain damage states incorporated with different level variances of mass density and Young's modulus.

3.6. Estimation of crack depth probability for variant systems with noised measured frequency

The severity identification process discussed in Sections 3.3 and 3.4 were for the property-invariant structure system and noise-free measured modal frequency. When the system mass density and stiffness were varied, the FCI simulation databases needed to extend. Basically, in the invariant system, for a specific damage state of structure, its frequency change was a certain value only; it will map to a certain and confirmed point on the FCI curve as shown in Fig. 2. But for a property-variant system, for a specific damage state, the property variations will cause the change of frequency varied; then the corresponding point on FCI curve will be "smeared" as shown in Fig. 5. Usually we use a distribution function to describe the smearing, for example, by a Gaussian distribution; and the noise-polluted measured modal frequency could also be described in a Gaussian distribution manner.

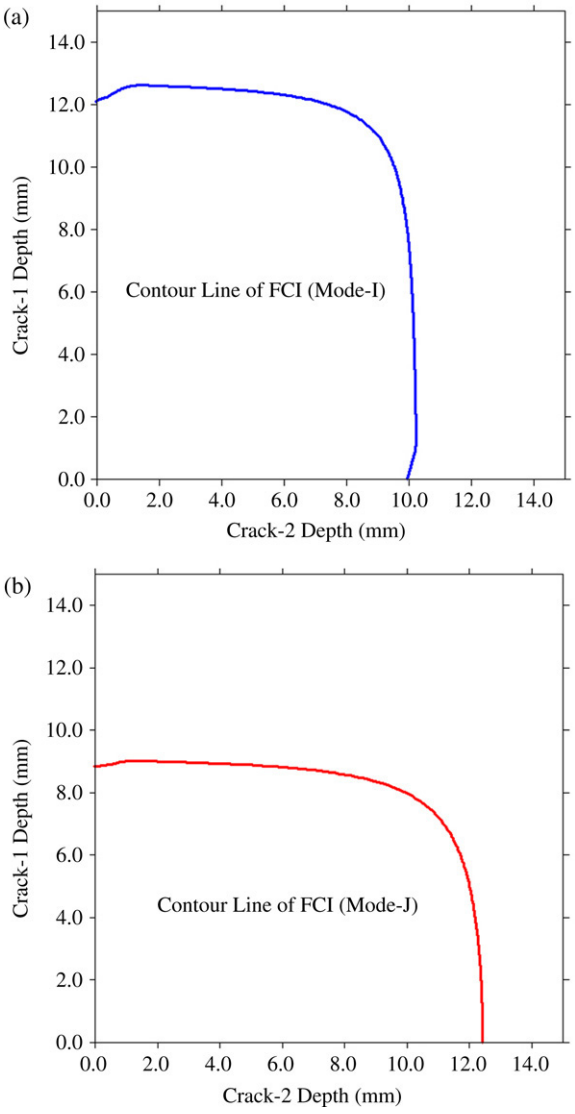

Fig. 3. FCI contour lines due to multiple crack existence: (a) contour line of mode I (b) contour line of mode J.

Since the FCI curve possesses a probability distribution characteristic in variant systems, the results of identification will also display the presence of a probability distribution. As shown in Fig. 5, in the statistical damage database, every point on the FCI curve was accompanied with a Gaussian distribution; when we applied the measured frequency by EMA in a probability distribution to find the unknown crack depths, we found that the probability distribution with mean value f_x was overlapped with several Gaussian distribution curves which represented different damage states (crack depth). Each overlapping represented the probability on these damage states. Hence, for a single noise-polluted measured frequency by EMA, we will have several possible crack depths with their probability. By collecting all the probabilities along various crack depths, the identified results will present a probability distribution curve.

Due to the measured frequency being noise polluted, we may represent its measured modal frequency by a probability distribution function. Assume that the material

property variation is independent of measurement noise. Each probability (P_i) at damage state i (crack depth) can be calculated by the following equation:

$$P_i = \int_{fa}^{fb} p_i(f)^* p^{\mathrm{EMA}}(f_x)\mathrm{d}f \tag{14}$$

where f_x was calculated by the mean of measured frequency, and $p_i(f)$ was the probability distribution function of the modal frequency in the simulation database for damage state i (crack depth), and the $p^{\mathrm{EMA}}(f_x)$ was the probability distribution function of the measured frequency with noise, and the upper bound and lower bound frequency fb, fa, should be determined by confidence level and the statistical t-test [8] that we discuss later in this section. Both of the $p_i(f)$ and $p^{\mathrm{EMA}}(f_x)$ were defined by the Gaussian distribution function $G(f)$ as below.

$$G(f) = \frac{1}{\sigma\sqrt{2\pi}} \exp\left[-\frac{1}{2}\left(\frac{f-\mu}{\sigma}\right)^2\right]. \tag{15}$$

The statistical t-test was used to assess the statistical significance of damage-sensitive features of EMA with the data in the simulated damage database. As stated above in this section, the upper and lower bound frequency of the probability function in Eq. (14) should be determined by confidence level and the statistical t-test. As described in Ref. [8], assigning two samples the population size n_1 and n_2 with sample mean $\overline{X}_1$ and $\overline{X}_2$ and standard deviation S_1 and S_2, a test statistic Z can be defined as Eq. (16) to describe the hypothesis $\overline{X}_1 - \overline{X}_2 = \alpha$,

$$Z = \frac{\overline{X}_1 - \overline{X}_2 - \alpha}{\sqrt{\frac{S_1^2}{n_1} + \frac{S_2^2}{n_2}}} \tag{16}$$

$$\left|\overline{X}_1 - \overline{X}_2\right| \le 0 \tag{17}$$

where n_1, n_2 should be large enough to invoke the central limit theory to satisfy the normal distribution assumption and α is an arbitrary constant, assumed to be 0.0 in this research. The authors then set up the hypothesis to test the statistical significance by Eq. (17). By solving Eq. (16), we can then state that there was approximately 99% confidence level of truth, if $|Z| \leqq 3.0$.

After we have assigned the confidence level to 99%, the upper and lower bound frequency of Eq. (14) can be determined by measuring the distance between the mean of the EMA data and the simulated database, which should not exceed three times the root sum squared of the standard deviations of EMA data and those from the simulated databases.

We may notice that the all the discussion above adopted the figure in the single-crack case; however, the algorithm described was suitable both for multiple-crack and single-crack examples. However, the statistical FCI was a function of one crack depth for the single crack; for the multiple-crack case the statistical FCI was a function of many depths at the specific locations identified.

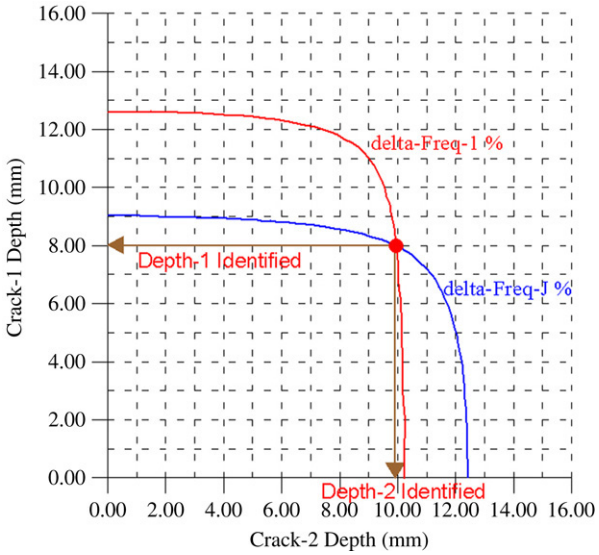

Fig. 4. To determine crack depths by the intersection of two FCI contour lines.

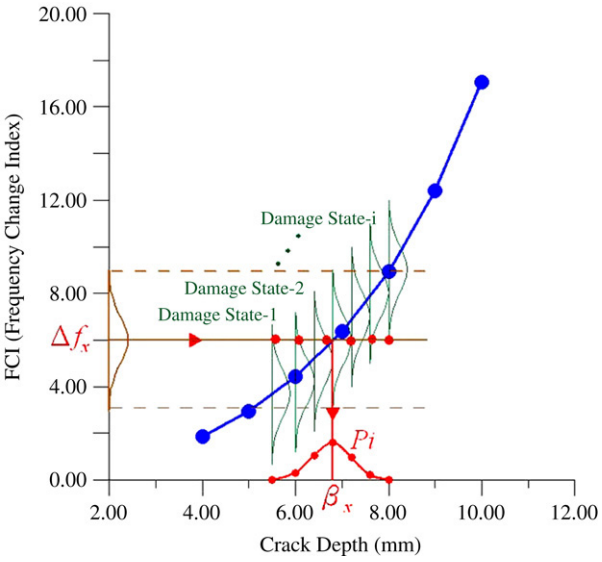

Fig. 5. Crack depth assessment for property variant system.

4. Procedures for crack detection and identification

Three major steps in the process flowchart shown as Fig. 6 and the procedures are described as follows.

4.1. Crack location detection

When we had prepared the modal frequency and mode shape of damaged beam from EMA and the modal frequencies and mode shapes of intact beam from simulation, by analyzing the peak response of LDI, we can identify crack location by Eq. (10).

4.2. Generate simulated statistical FCI database

Since we had obtained the crack locations of the damaged beam, building up the damage severity database should be followed. For the property-variant system, we need to describe

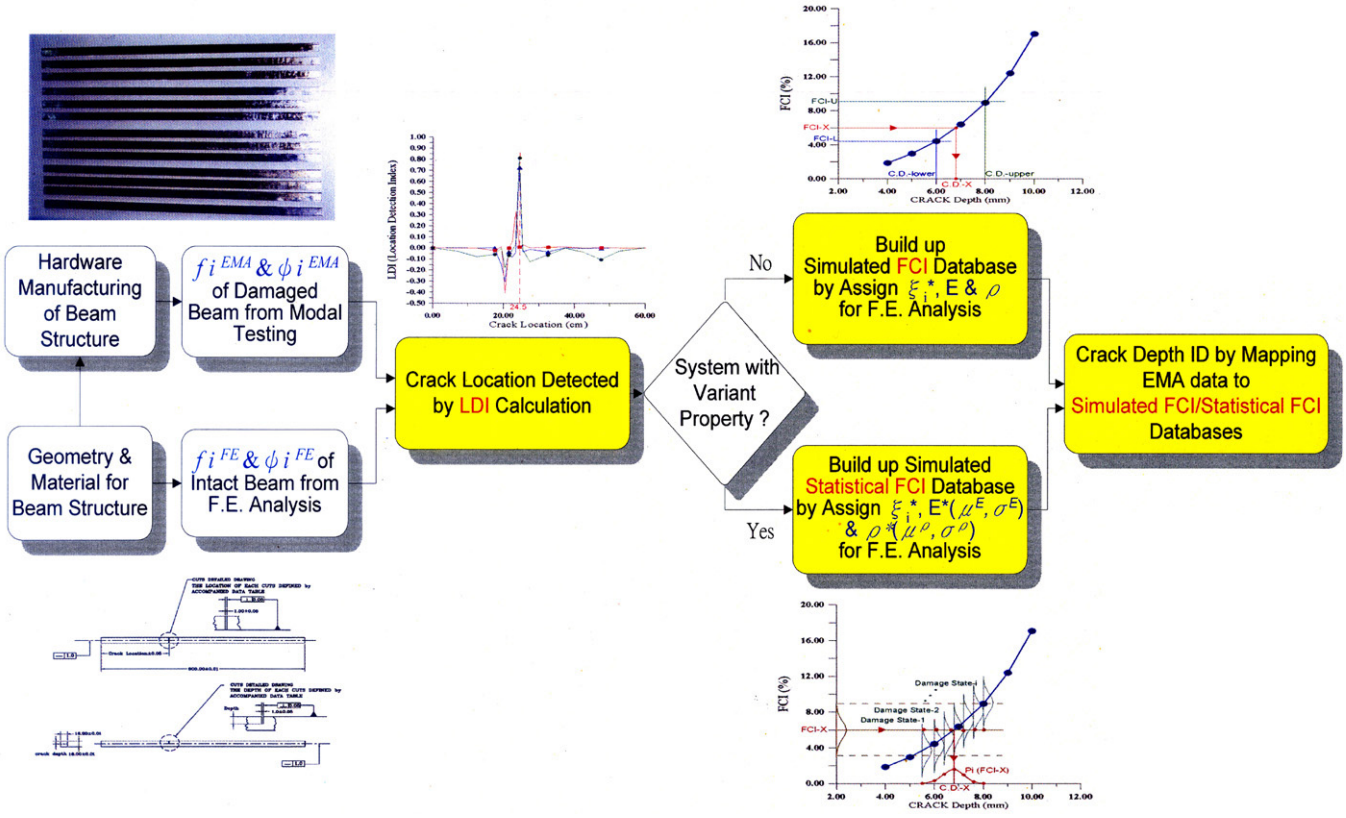

Fig. 6. Flowchart of crack assessment procedures of beam structure.

the property variation in the form of mean and standard deviation of a Gaussian distribution. By using the LHS sampling technique [11,19], we shall have a minimum number of useful samples that are incorporated with various E^*, ρ^* and ξ_i^*. E^* and ρ^* were specific variation values of stiffness and mass density randomly selected by LHS sampling, and the ξ_i^* denoted the specific depth of cracks from a series of possible crack depths. By assigning each set that composed of ξ_i^* with E^* and ρ^* for finite element normal mode analysis repeatedly, we could generate the simulated statistical FCI databases represented by its modal frequency and variation among various crack depths. The above process is called Monte Carlo simulation.

The same procedures were used for the property-invariant system to generate a simulated FCI database, except that for the deterministic system, there was no need to do Monte Carlo simulation due to the stiffness (E) and mass properties (ρ) that were all fixed with no variance. It required only doing the deterministic normal mode analysis for one set of specific crack depths (ξ_i^*) among the possible crack depths to build the database.

4.3. Identify crack depth

For the variant system, by assigning confidence level to approximate 99%, then the statistical significance of the damage level was examined by t-test, and the upper and lower bounds of integration in Eq. (14) were then determined. Since we have built the simulated statistical FCI databases for a property-variant system, we can map the noised measured frequency by EMA to the data of simulated databases that were both represented in Gaussian distribution form, then the crack depths were assessed by probability.

5. Demonstration examples

The damaged beam (Beam-I) was used to demonstrate the assessment of a single-crack beam with different measurement resolution. A single shallow depth cracked beam (Beam-N) was also used to test the capability of the proposed method. A multiple-crack example was represented by a two-crack beam (Beam-M); the assessment process was demonstrated as follows:

5.1. Crack location detect of Beam-I

From the finite element normal mode analysis and EMA data, we have the three lowest mode shapes of the damaged beam and intact beam. The crack location can be detected by applying the LDI by Eq. (10) in Section 3.1. By reviewing the results in Fig. 7(a), we found that the crack was located at 245 mm by the peak of LDI curve of mode 1 and 3; by mode 2 the crack was located at 235 mm. When compared to the real crack location 243 mm, the averaged absolute error was 1.64%.

5.2. Crack depth identification of Beam-I for property non-variant system

As discussed in Section 4 and the procedures shown in Fig. 6, for a property non-variant system, we had built the

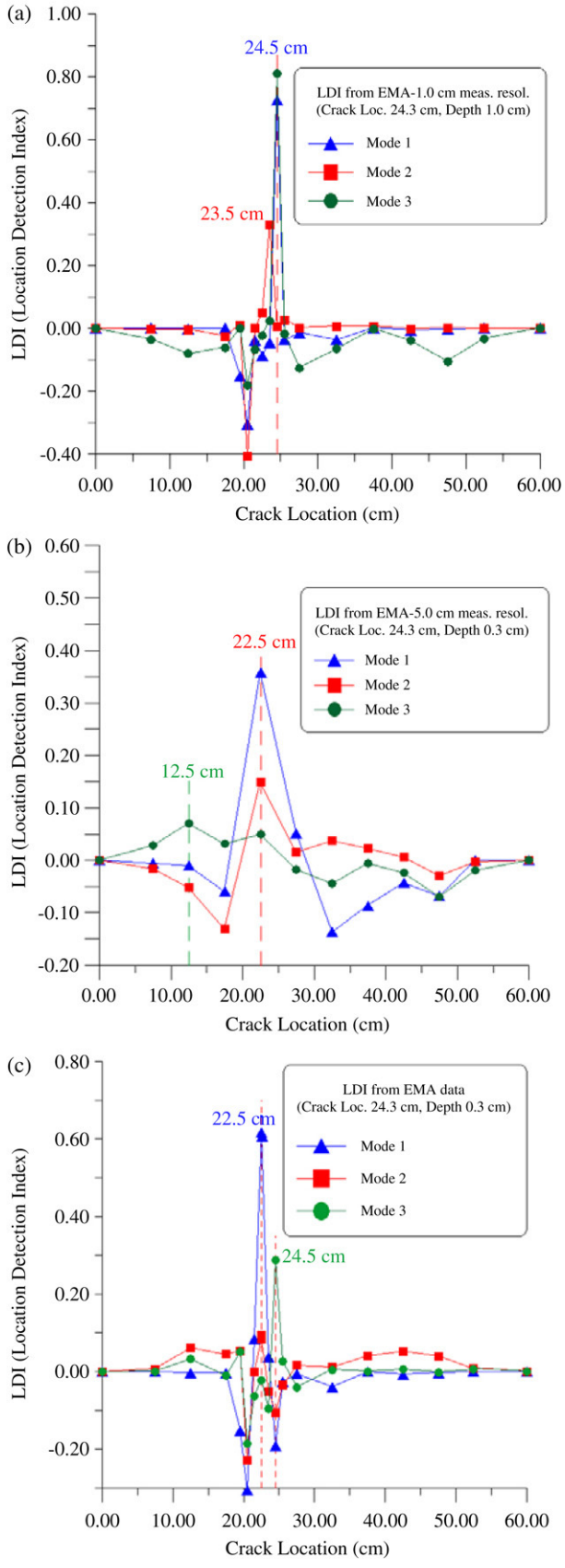

Fig. 7. Crack location detect by LDI curve (a) Beam-I, meas. resol. 10 mm (b) Beam-I, meas. resol. 50 mm (c) Beam-N, meas. resol. 10 mm.

simulated FCI database according to the crack location 245 mm that was determined in the previous section. Then the unknown crack depth can be identified by Eq. (13). Since we had the EMA measured frequencies that were 193.43 Hz, 602.38 Hz and 1210.66 Hz for the lowest three modes, by the interpolating process as shown in Fig. 8, we have crack depth 10.02 mm, 10.26 mm and 9.66 mm for the three lowest modes respectively. The errors were +0.2%, +2.6% and −3.4% for the three modes and the averaged absolute error was 2.07%.

5.3. Crack depth identification of Beam-I for property variant system

For a property-variant system, refer to procedures described in Section 4 and procedures shown in Fig. 6, we need to build the simulated statistical FCI database according to the crack location found in Section 5.1. In order to build the statistics database, we assumed the variations of mass density & Young's modulus were ±2%, ±5% and ±10% of its mean value. By sensitivity analysis, 300 samples were used for LHS sampling. The typical data from Monte Carlo simulation results on certain crack depth with different level of variations for different modes are shown in Table 2. Each set of mean with standard deviation represented a probability distribution on a point (crack depth) of statistical FCI curve as shown in Fig. 5.

Although the experiments were controlled in the laboratory, there still was variability in the experimental data. For the study of noised measured frequency effects, the authors assumed that we have noise on the measured frequencies. The variations of noised frequency were assumed as ±2%, ±5% and ±10% of measured frequency incorporated with ±2%, ±5% and ±10% material variations. With Eq. (14) we could assess the probability of specific severity by mapping the measured frequency to each of the probability distribution curves of the statistical FCI database. By changing to different depths in sequence, we have probabilities at all depths.

The interpreted probability distributions of crack depth on material variations and varied noise level measured frequency are shown in Fig. 11. We have observed that from mode 1 results (1st row in Fig. 11), for 2% and 5% material variation, the maximum probability of crack depth occurred at 10.0 mm for 0%, 2%, 5% and 10% measured frequency noise, and for 10% material variation, the maximum probability of crack depth occurred at 10.25 mm for 0%, 2%, 5% and 10% noise in the measured frequency. From mode 2 data (2nd row in Fig. 11), only results for 2% and 5% material variation with measured frequency noise less than 2% can be identified; the maximum probability of depth occurred at 10.25 mm. From data for mode 3 (3rd row in Fig. 11), only the results of the material variation and noised measured frequency both less than 2% can be identified; the maximum probability of crack depth occurred at 9.75 mm.

By reviewing Fig. 11 again, we found data in the first mode; the crack depth has a distinct peak and the narrowest spread of its probability distribution. This means that the lowest mode has less scattering on severity identification. We have also found that both the larger material variation and the

Table 2
Monte Carlo simulation results among various crack depths (Beam-I)

Depth of crack (mm)	Variant level of mass density & Young's modulus (in % of mean)	Mode-1 (Hz)		Mode-2 (Hz)		Mode-3 (Hz)	
		Frequency	Standard deviation	Frequency	Standard deviation	Frequency	Standard deviation
9.00	2	205.20	2.93	613.3	8.75	1217.0	17.35
	5	205.30	7.35	613.6	21.96	1217.0	43.57
	10	205.70	14.89	614.8	44.50	1220.0	88.29
9.50	2	200.10	2.85	609.0	8.69	1211.0	17.28
	5	200.30	7.17	609.3	21.81	1212.0	43.38
	10	200.60	14.52	610.5	44.19	1215.0	87.91
9.75	2	197.30	2.81	606.6	8.65	1209.0	17.24
	5	197.40	7.06	606.9	21.72	1209.0	43.28
	10	197.80	14.31	608.1	44.02	1212.0	87.70
10.00	2	194.30	2.77	604.2	8.62	1206.0	17.19
	5	194.40	6.96	604.6	21.64	1206.0	43.17
	10	194.80	14.10	605.7	43.85	1209.0	87.49
10.25	2	190.90	2.72	601.6	8.58	1202.0	17.15
	5	191.00	6.84	601.90	21.54	1203.0	43.06
	10	191.40	13.85	603.10	43.66	1205.0	87.25
10.50	2	187.30	2.67	598.9	8.54	1199.0	17.10
	5	187.40	6.71	599.3	21.45	1200.0	42.94
	10	187.80	13.59	600.4	43.46	1202.0	87.01
11.00	2	179.40	2.56	593.3	8.46	1192.0	17.00
	5	179.50	6.42	593.7	21.25	1193.0	42.68
	10	179.80	13.02	594.8	43.06	1195.0	86.50

larger noise level of the measured frequency will make the probability distribution wider on severity and the reliability will be decreasing on the depths which had been identified.

5.4. The measurement resolution effects on assessment results

The above example was based on the assumption that we have the appropriate number of measurements; the authors took 10 mm as the spacing between measurement points near the crack zone and 50–75 mm on the others: 18 impact locations in total. In this section, in order to test for the effectiveness of the proposed algorithm, the measurement spacing was extended to 50–75 mm for the entire beam: 12 impact locations in total. According to the result of EMA and finite element normal mode analysis, the crack location can be detected as shown in Fig. 7(b). From the peak of LDI curve of mode 1 and 2 we found that the crack was located at 225 mm (−7.4% error). From mode 3 we have the crack located at 125 mm (−48.6% error). Mode 3 data lost its accuracy and it cannot be used for further identification on depth. With compared to the results of 18-impact measurement resolution (1.64% error), we have less accuracy of crack location due to the larger measurement spacing.

For the property-invariant system, we took mode 1 and mode 2 results (crack location 225 mm) as the basis to generate the FCI database. With the same procedures described in the above example, by the interpolating process as shown in Fig. 9, the crack depth was identified by FCI: we have 10.26 mm (+2.60% error), 8.50 mm (−15.0% error) in crack depth for the first and second mode respectively. Compared to the results of the above 18-impact measurement resolution example, its averaged absolute error of the lowest three modes (2.07%) shows that we have less accurate results on crack location. Besides, due to the FCI database being based on crack location 225 mm, the location was very close to one of the nodes of curvature mode shape 3; hence we have a poor result when applying mode 3 data for crack assessment.

For the property-variant system with noised measurement, the statistical FCI database was also based on mode 1 and mode 2 results. For various property variation and different levels of measurement noise, the crack depth was determined by the highest probability. The assessed probability distribution is shown in Fig. 12. From mode 1 results (1st row in Fig. 12), for 2%, 5%, 10% and material variation, the maximum probability of crack depth occurred at 10.25 mm for all levels of measurement noise. From mode 2 data (2nd row in Fig. 12), only results for 2% and 5% material variation with measurement noise less than 2% can be identified for crack depth; its maximum probability occurred at 8.50 mm. From mode 3 data (3rd row in Fig. 12), there was no clear indication for crack depth due to the crack location used for statistical FCI database being very close to one of the nodes of curvature mode shape 3. Compared to the results of the 18-impact measurement resolution example, with 0.83% error for mode 1 and 2.5% error for mode 2 and 3, we have less accurate results on crack depth identification.

By reviewing Fig. 12, we have the same conclusion as with the example of 18-impact measurement resolution: the result from first mode has a distinct peak and the narrowest spread

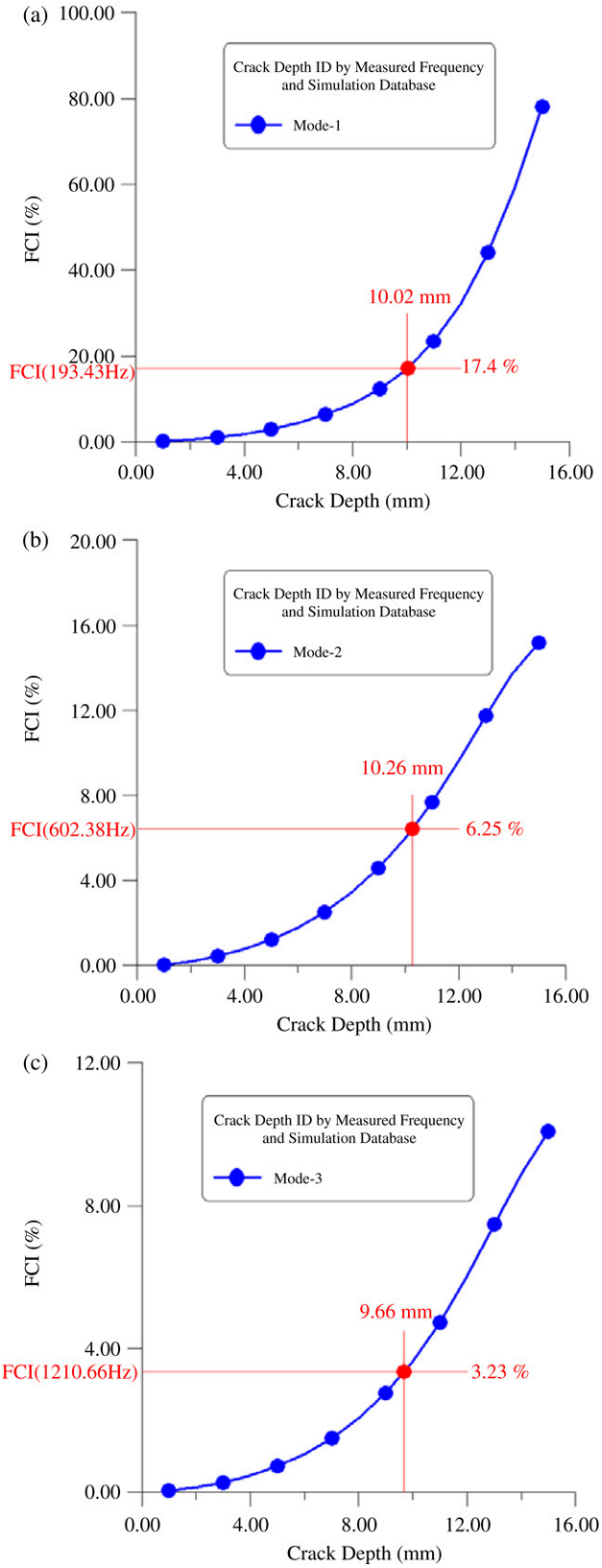

Fig. 8. Crack depth identification by FCI (Beam-I, meas. resol. 10 mm, crk. loc. 243 mm, depth 10 mm) (a) mode 1 (b) mode 2 (c) mode 3.

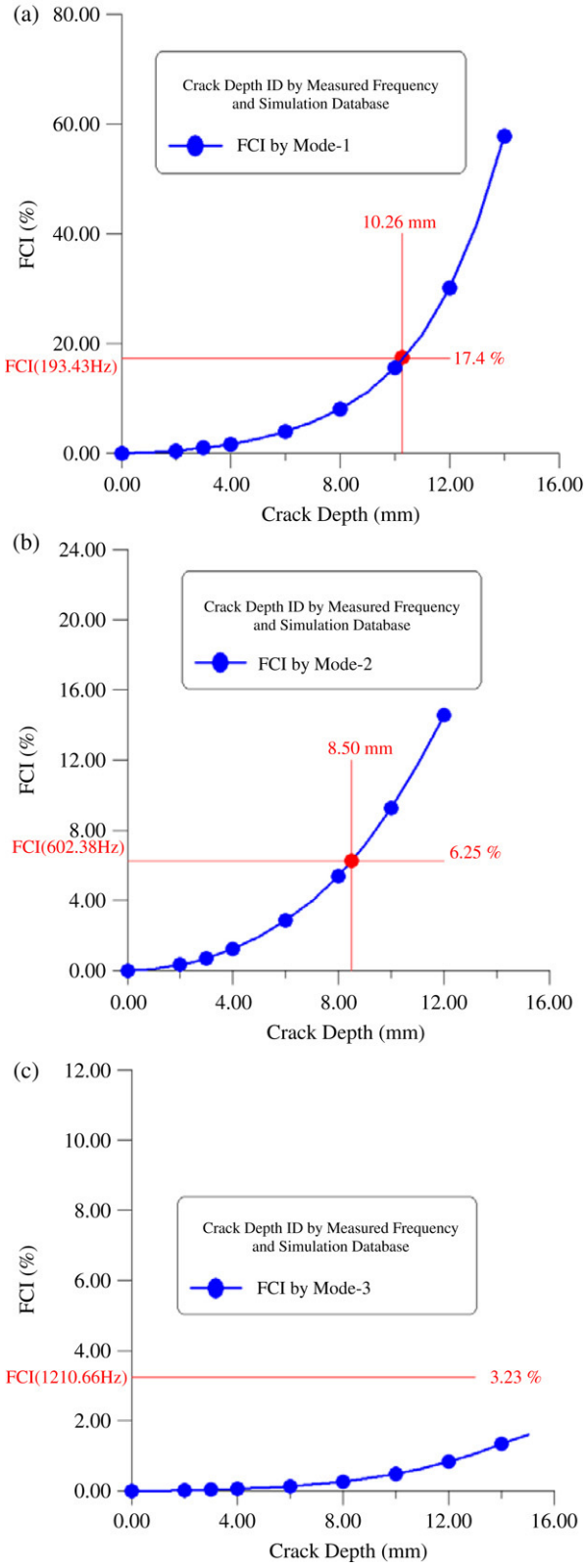

Fig. 9. Crack depth identification by FCI (Beam-I, meas. resol. 50 mm, crk. loc. 243 mm, depth 10 mm) (a) mode 1 (b) mode 2 (c) mode 3.

of its probability distribution on severity. The higher the mode used in assessment, the larger the material variation or the larger the noise level of the measured frequency will make the error larger, the probability lower and the distribution wider.

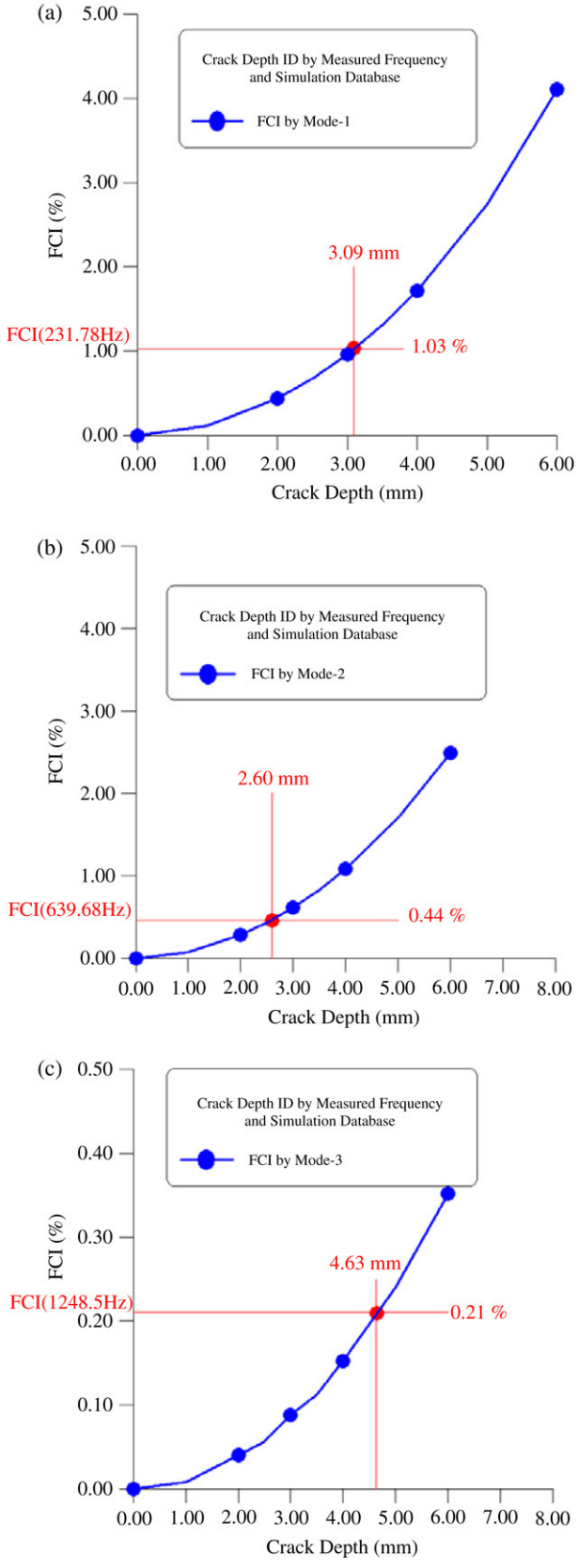

Fig. 10. Crack depth identification by FCI (Beam-N, meas. resol. 10 mm, crk. loc. 243 mm, depth 3 mm) (a) mode 1 (b) mode 2 (c) mode 3.

5.5. The shallow crack depth example (Beam-N case)

It is always challenging work to identify a small depth crack in a structure. A sample beam, named as Beam-N, was designed to complete the study. For the convenience of comparing with the Beam-I example, a cracked beam was manufactured by a wild-cut with the same crack location 243 mm but a smaller crack depth 3 mm.

According to the finite element normal mode analysis result and EMA data (by 10 mm measurement resolution near the crack, 18-impact example), the crack location can be detected as shown in Fig. 7(c). From the peak of LDI curve of mode 1 and 2, we found that the crack was located at 225 mm (−7.41% error) and from mode 3 we have the crack located at 245 mm (+0.82% error). The averaged absolute error was 5.21%; compared to the results of Beam-I we have larger error for a small crack depth beam example in crack location detection.

For the identification of shallow-depth cracked beam in the property-invariant system, the authors took the average of mode 1 and mode 2 results (averaged crack location 232 mm) as the basis to generate the FCI database. With the same procedures as Beam-I, we had the EMA measured frequencies 231.78 Hz, 639.68 Hz and 1248.47 Hz for the lowest three modes; by the interpolating process as shown in Fig. 10, the crack depth was identified by FCI as 3.09 mm (+3.0% error), 2.60 mm (−13.3% error), and 4.63 mm (+54.3% error) for mode 1, mode 2 and mode 3, respectively; only the mode 1 result was acceptable in accuracy. However, the small denominator (crack depth 3.0 mm) made the large relative error. If we take a look at its absolute error, 0.09 mm, 0.40 mm, 1.63 mm for mode 1, 2 and 3, compared to the result for Beam-I, 0.02 mm, 0.26 mm and 0.34 mm, they were at the same error level except for mode 3. But, due to the large denominator (crack depth 10.0 mm) we will have smaller absolute error for Beam-I.

For the crack depth identification of the property-variant system with noised measured frequency, the statistical FCI database was based on mode 1 and mode 2 results (crack location 232 mm). The results of probability distribution assessment are shown in Fig. 13. We have observed that only the crack depth can be identified, by mode 1 under 2% material variations with no measurement noise, and the crack depth is identified as 3.20 mm (+6.67% error) by the highest probability. Compared to the results of Beam-I (10 mm crack depth), its crack depth was 0.83% error for mode 1 and 2.5% error for modes 2 and 3; we have less accurate results on crack depth identification. We have found that first-mode result for Beam-N does not have a sharp peak and a narrow spread of its probability distribution. The probability distribution for mode 1 has the same shape as the higher mode with higher measurement noise in Figs. 11 and 12.

5.6. The multiple-crack example (Beam-M case)

The assessment of the above examples was all based on the single-crack configuration. Multiple cracks may exist in structure systems. In this section, the multiple-crack sample (named Beam-M) was adopted to test for the effectiveness of

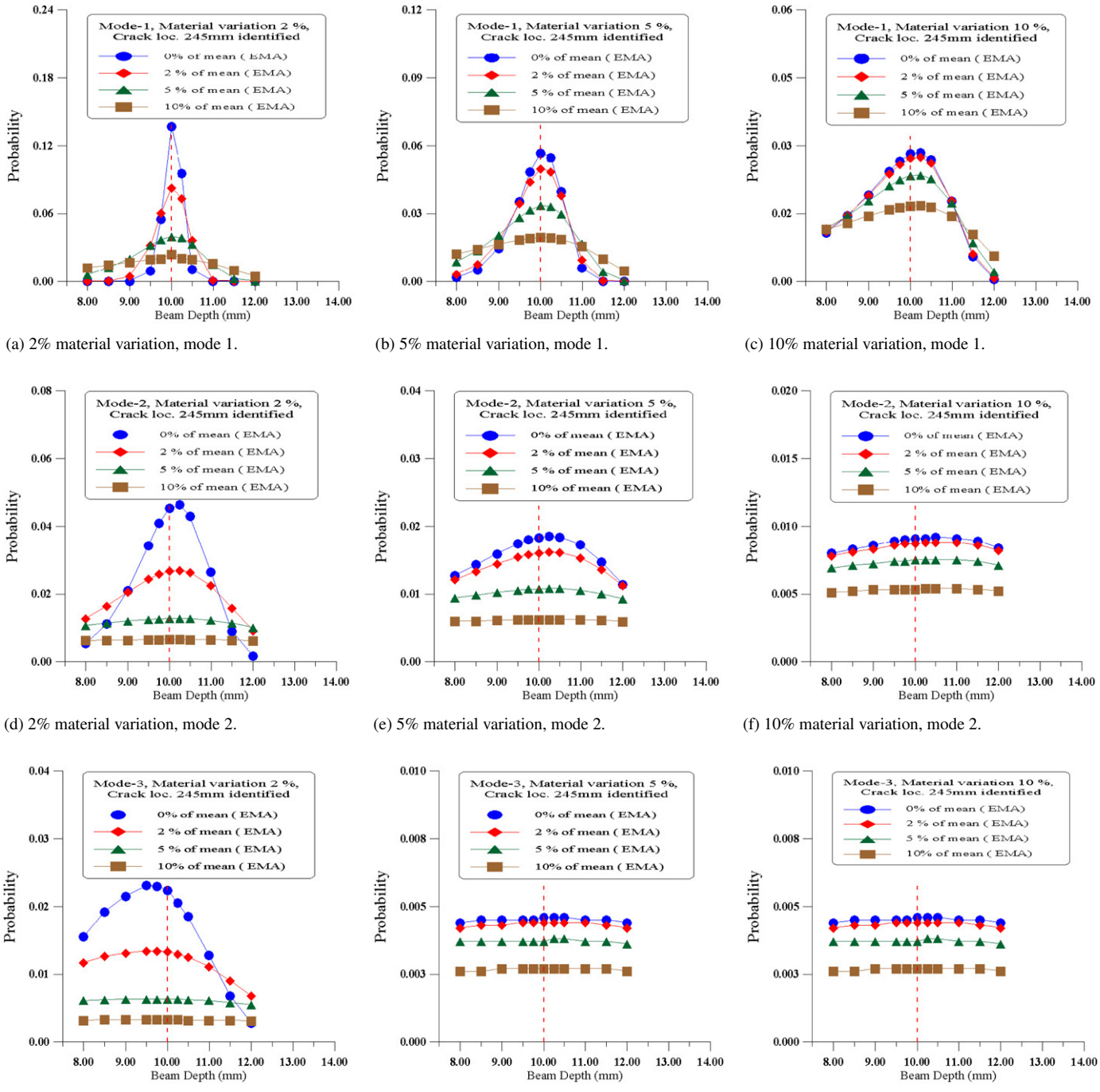

(a) 2% material variation, mode 1. (b) 5% material variation, mode 1. (c) 10% material variation, mode 1.

(d) 2% material variation, mode 2. (e) 5% material variation, mode 2. (f) 10% material variation, mode 2.

(g) 2% material variation, mode 3. (h) 5% material variation, mode 3. (i) 10% material variation, mode 3.

Fig. 11. Probability distribution of Beam-I among varied crack depth (meas. resol. 10 mm; 1st column for 2%, 2nd column for 5%, 3rd column for 10% material variation and 1st row for mode 1 data, 2nd row for mode 2 data, 3rd row for mode 3 data respectively).

the proposed algorithm. For convenient comparison with Beam-I, the authors made an extra crack on Beam-I; it was also manufactured by wild-cut at a new crack location 131 mm with the crack depth 8 mm. Beam-M then has two cracks on its configuration; the first crack is located at 131 mm, with depth 8 mm, and the second crack is located at 243 mm, with depth 10 mm.

According to the finite element normal mode analysis result and EMA data, the cracks' location can be detected as shown in Fig. 14. From the peak of LDI curve of the mode1 and 3; we found the cracks were located at 135 mm (+3.05% error) and 245 mm (+0.82% error), and there were different sensitivities on the peak of LDI for various modes. The averaged absolute error of the multiple-crack case was equal to +1.94%. Compared to Beam-I case (1.64% error), we have the same error level in crack location detection.

We applied the identified multiple-crack location by LDI for FCI database generation (crack locations 135 mm and

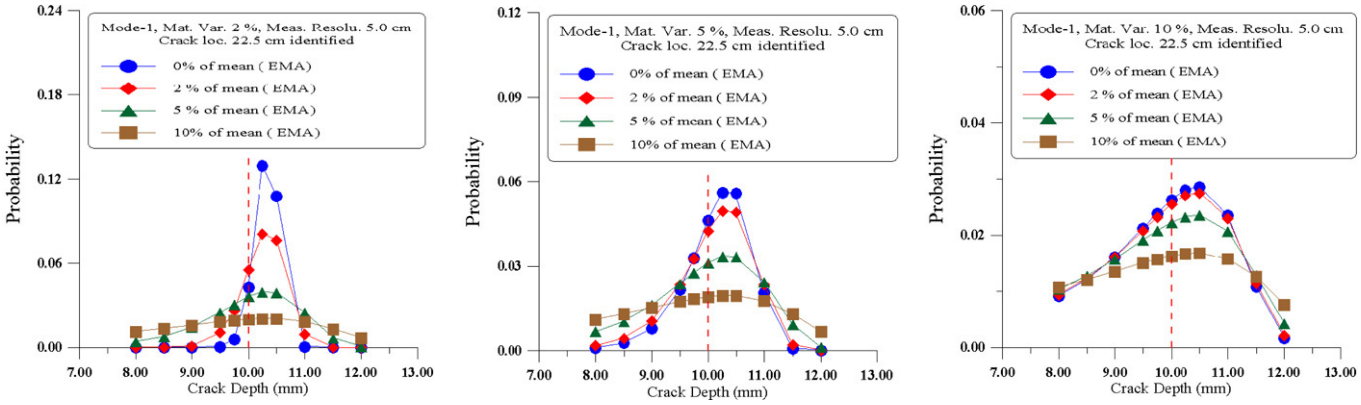

(a) 2% material variation, mode 1. (b) 5% material variation, mode 1. (c) 10% material variation, mode 1.

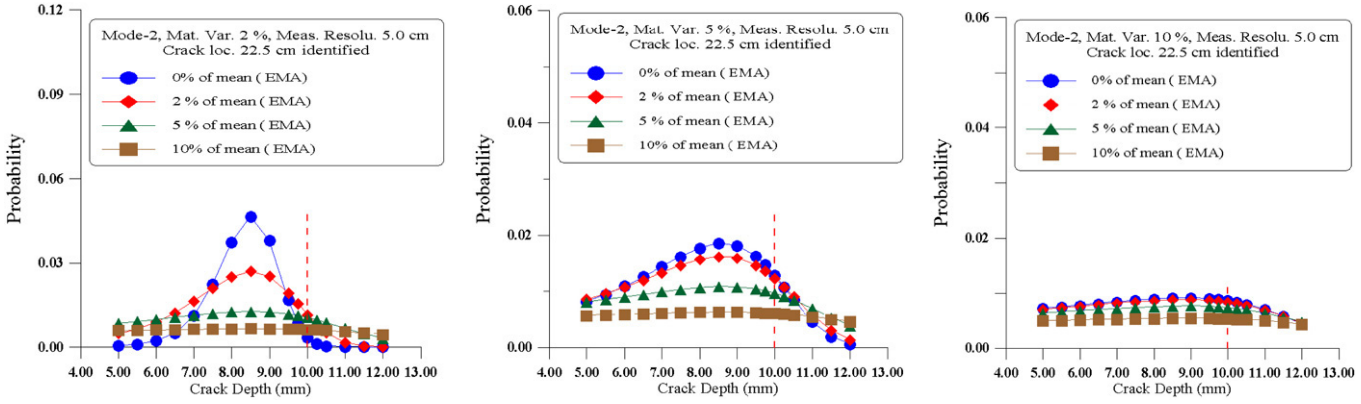

(d) 2% material variation, mode 2. (e) 5% material variation, mode 2. (f) 10% material variation, mode 2.

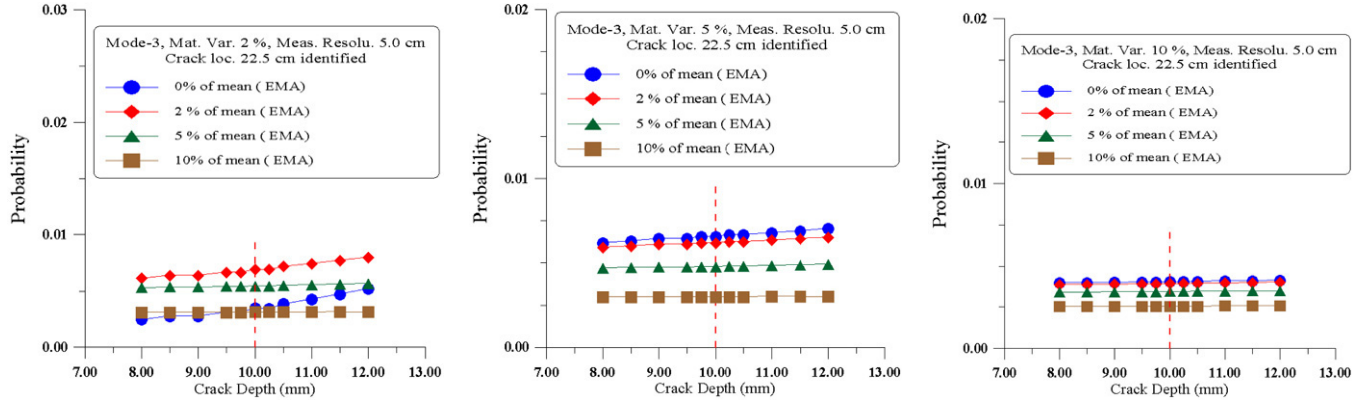

(g) 2% material variation, mode 3. (h) 5% material variation, mode 3. (i) 10% material variation, mode 3.

Fig. 12. Probability distribution of Beam-I among varied crack depth (meas. resol. 50 mm; 1st column for 2%, 2nd column for 5%, 3rd column for 10% material variation and 1st row for mode 1 data, 2nd row for mode 2 data, 3rd row for mode 3 data respectively).

245 mm). From EMA we have the first three modal frequencies 191.25 Hz, 574.83 Hz and 1079.46 Hz of Beam-M, and also from finite element analysis for the no-damage beam (Beam-S); its modal frequencies were 234.19 Hz, 642.53 Hz and 1251.1 Hz. We have frequency changes of 18.34%, 10.54%, 13.72% for the three modes, respectively. We need 2 sets of FCI curves to identify the depths due to the frequency change dominated by multiple cracks simultaneously. A little modification is needed in comparison to the single-crack case: we should first plot the contour lines of the frequency change on each mode, as shown in Fig. 15. Then by the intersection operation of two contour lines from different modes, as shown in Fig. 16, the crack depths were identified as 8.00 mm (0.0% error) and 9.90 mm (+1.00% error) by the first and second mode or by the first and third mode. The averaged absolute error for the depths of multiple cracks was equal to 0.50%. With

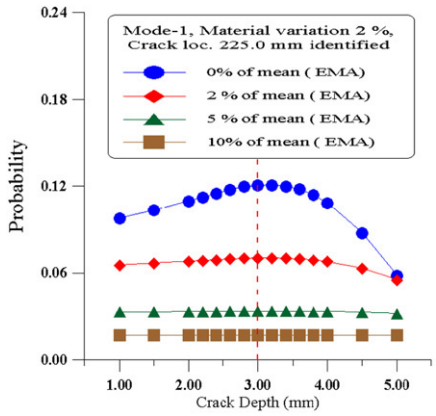

(a) 2% material variation, mode 1.

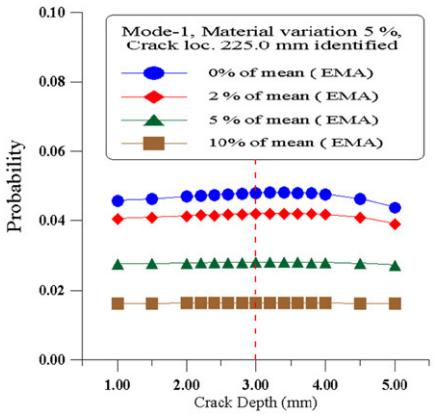

(b) 5% material variation, mode 1.

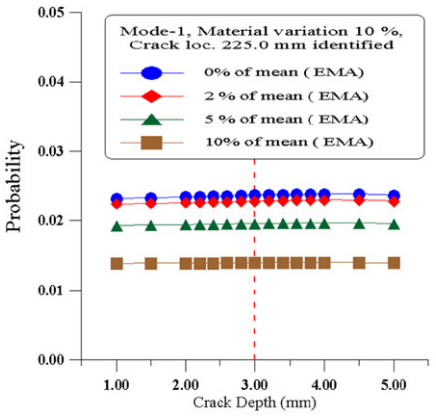

(c) 10% material variation, mode 1.

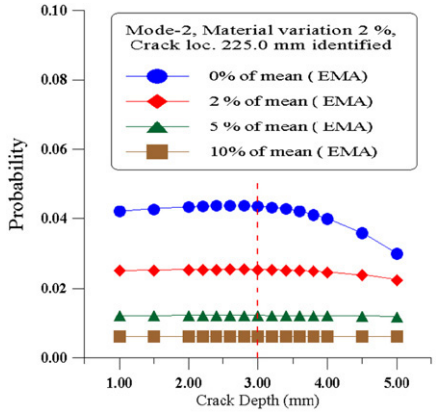

(d) 2% material variation, mode 2.

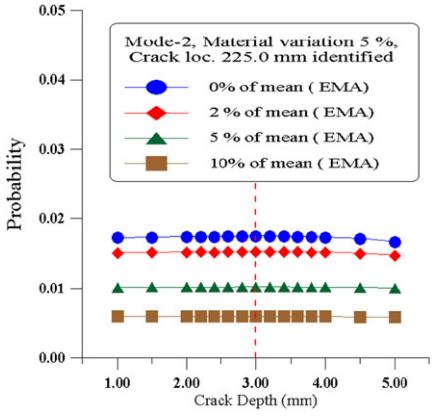

(e) 5% material variation, mode 2.

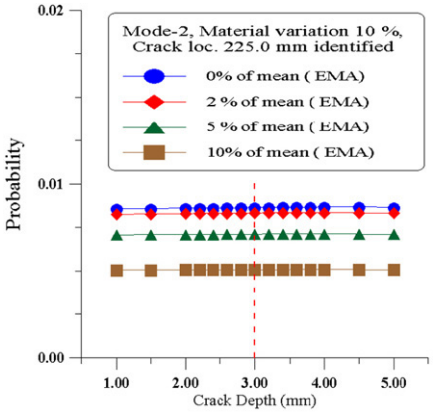

(f) 10% material variation, mode 2.

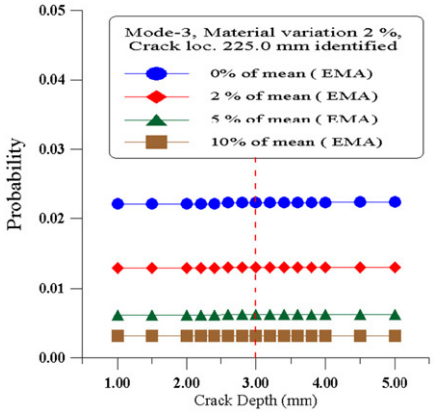

(g) 2% material variation, mode 3.

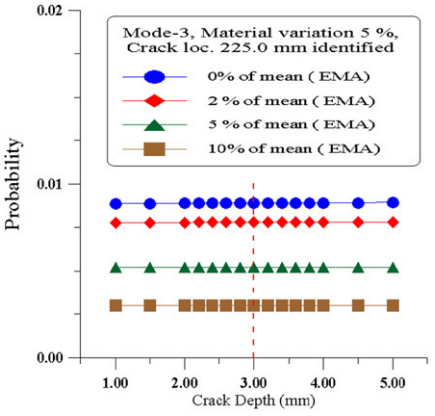

(h) 5% material variation, mode 3.

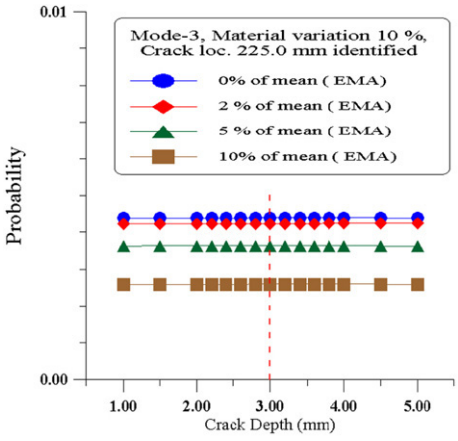

(i) 10% material variation, mode 3.

Fig. 13. Probability distribution of Beam-N among varied crack depth (crk. loc. 243 mm, depth 3 mm, meas. resol. 50 mm; 1st column for 2%, 2nd column for 5%, 3rd column for 10% material variation and 1st row for mode 1 data, 2nd row for mode 2 data, 3rd row for mode 3 data respectively).

compared to the results of Beam-I (2.07%), we also have the same error level on depth identification for the multiple-crack case for the invariant system.

For the variant system with noised measurement, the statistical FCI database was also based on the cracks located at 135 mm and 245 mm that were detected by peak LDI. Various property variation and different level measurement noise were applied, and the crack depths were determined by the highest probability. As mentioned above, due to the frequency change being dominated by multiple cracks simultaneously, we will determine all the depths at the same time. The probability of identified crack depths was represented by its brightness; the higher the probability, the brighter it was, and vice versa. A red point in the figure indicated the highest probability on the

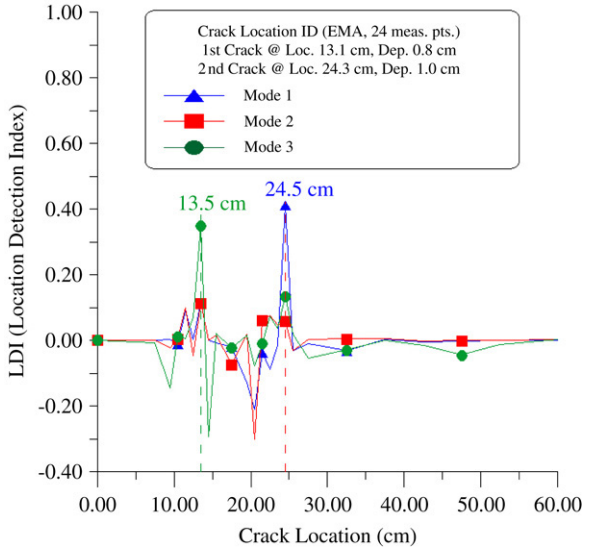

Fig. 14. Multiple-crack location detected by LDI (crk-1 loc.131 mm, crk-1 dep. 8 mm, crk-2 loc.243 mm, crk-2 dep. 10 mm).

depths. The assessed probability distributions of depths are shown in Figs. 17–19 for modes 1, 2 and 3 respectively. The identified depths and averaged absolutely error are listed in Table 3.

Results from mode 1 as shown in the 1st column (2% material variation) and the 2nd column (5% material variation) in Fig. 17, its maximum probability of cracks' depth occurred at 8.50 mm and 9.90 mm for all levels of measurement noise. The maximum probability of cracks' depth occurred at 7.57 mm and 10.15 mm for all levels of measurement noise for 10% material variation as shown in the 3rd column in Fig. 17. In the 1st row of Table 3, we have found that their averaged absolute errors were ranged from 3.44% to 3.63% for mode 1. Compared to the Beam-I single-crack case (0.83% error for mode 1), we have acceptable error on the crack depth identified.

From mode 2 results, for 2% material variation (1st column in Fig. 18), the maximum probability of crack depth occurred at 7.50 mm and 10.77 mm for 0% and 2% measurement noise, and the crack depth occurred at 8.25 mm and 9.47 mm for 5% and 10% measurement noise. For 5% material variation (2nd

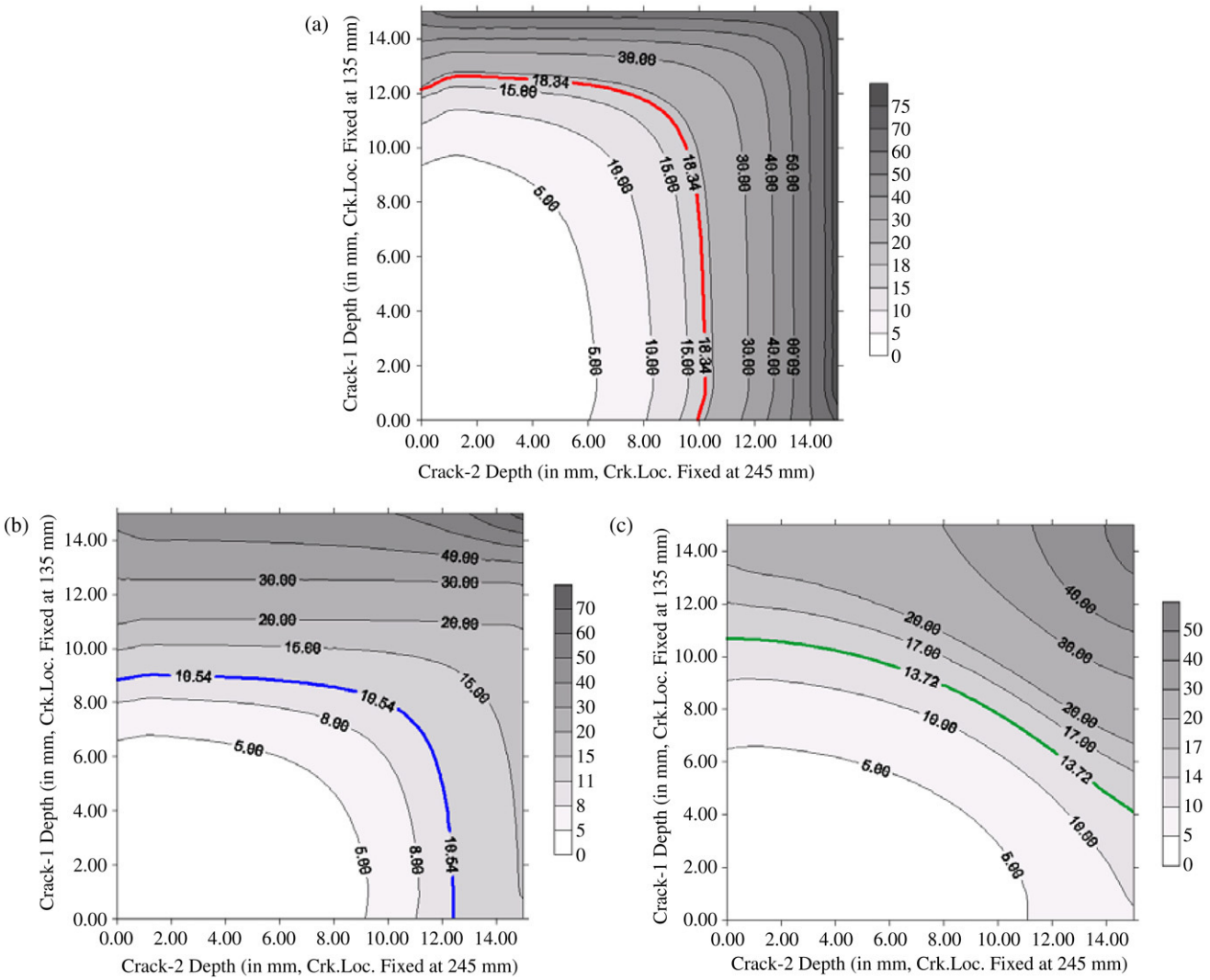

Fig. 15. FCI contour lines due to multiple-crack existence: (a) mode 1 (18.34%), (b) mode 2 (10.54%), (c) mode 3 (13.72%).

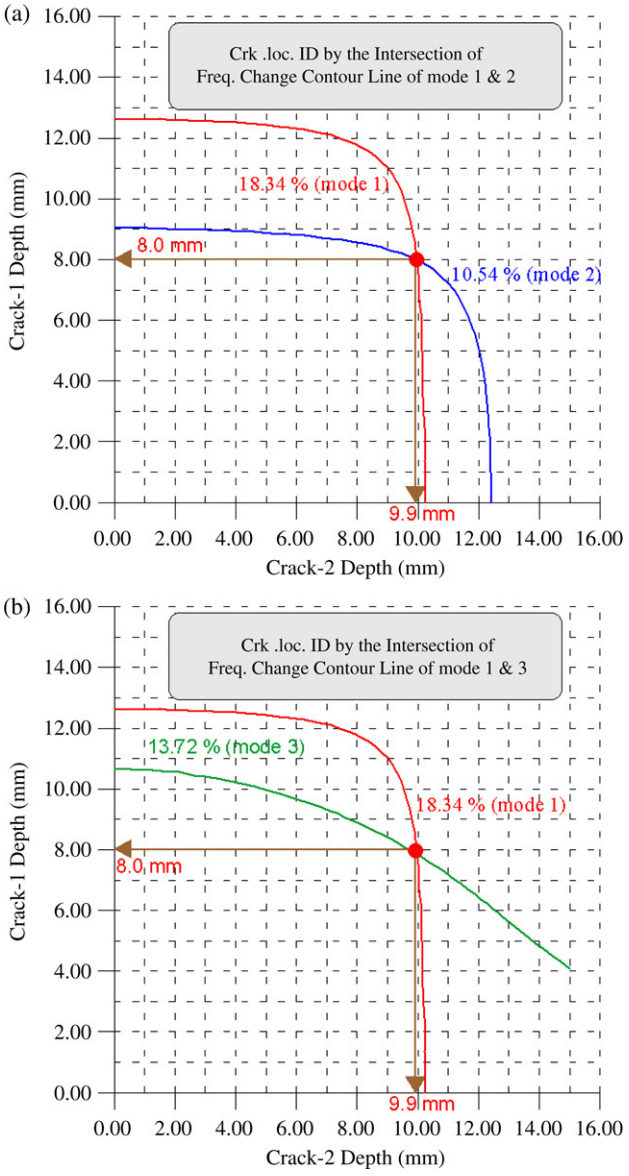

Fig. 16. Crack depths Identification by the intersection of two FCI contour lines (a) by mode 1 and 2 (b) by mode 1 and 3.

column in Fig. 18), the maximum probability of crack depth occurred at 8.25 mm and 9.47 mm for all levels of measurement noise. For 10% material variation (3rd column in Fig. 18), the maximum probability of crack depth occurred at 8.25 mm and 10.33 mm for all levels of measurement noise. In the 2nd row of Table 3, we found that their averaged absolute errors were ranged from 3.21% to 6.98% for mode 2. With compared to the Beam-I single-crack case (2.50% error for mode 2), we also have acceptable error on the crack depths identified.

From mode 3 results, for 2% material variation (1st column in Fig. 19), the maximum probability of crack depth occurred at 7.75 mm and 10.33 mm for all levels of measurement noise. For 5% material variation (2nd column in Fig. 19), the maximum probability of crack depth occurred at 8.50 mm and 9.03 mm for 0%, 2%, and 5% measurement noise, and it occurred at 8.25 mm and 9.47 mm for 10% measurement noise. For 10% material variation (3rd column in Fig. 19), the maximum probability of crack depth occurred at 7.00 mm and 11.63 mm for all levels of measurement noise. In the 3rd row of Table 3, we found that their averaged absolute errors were ranged from 3.21% to 14.40% for mode 3. With compared to the Beam-I single-crack case (2.50% error for mode 3), we have the larger error on the crack depth identified.

Looking at Figs. 17–19, we have the same conclusion that the result from the lower mode, the lower material variant and the lower noise in measurement will have the brightest (sharpest) peak and the narrowest spread of its probability distribution on crack depth identification.

6. Conclusions and discussions

From the presented research, we have conclusions as follows:

(1) A damage assessment algorithm was developed for a beam with single and multiple cracks in a uniform mass density and Young's modulus variations system incorporated with different level noise in the measured modal frequency. The effects on measurement resolution and the shallow-depth crack were also investigated.

(2) Due to the material variation of the beams were varied uniformly across the entire beam, the LDI for crack location detection was held for both the property-variant and property-invariant systems. For the middle-depth single-crack beam (Beam-I, 10/16 depth of structure) we have the averaged absolute error 1.64% on the basis of measurement resolution 1/60 in beam length near the crack zone and 5/60–7.5/60 on the others, there were 18 impact locations in total.

(3) The crack depth was determined by the FCI or the statistical FCI database. For the middle-depth single-crack beam (Beam-I) with appropriate measurement spacing, we have the averaged absolute error 2.07% for the invariant system and 1.94% error for variant system with material variation, and measurement noise less than 10%.

(4) For practical applications, the "fixed response" method of EMA should be change to "fixed impact" to save labor work. It would be adequate to use a non-uniform spacing between measurement points and apply 1%–2% spacing in beam length close to the crack, and 8%–13% in spacing for the others. To increase the spacing from 1/60 (Beam-I) to 5/60 (Beam-N) in beam length on the crack zone, the error will be increased to 4.52 times in crack location detection, to 4.25 times in crack depth for the property-invariant system, and to 4.51 times in depth for the property-variant system.

(5) For the shallow crack depth single-crack example (Beam-N, 3/16 depth of structure), the LDI works well for location detection. Compared to the result of the middle-depth single-cracked beam (Beam-I, 10/16 depth of structure), the error will be increased to 3.18 times in location detection, and to 5.82 times in depth identification for the property-invariant system by mode 1 and mode 2 data, and to 3.44 times for the property-variant system by mode 1 data under 2% material variations with no measurement noise.

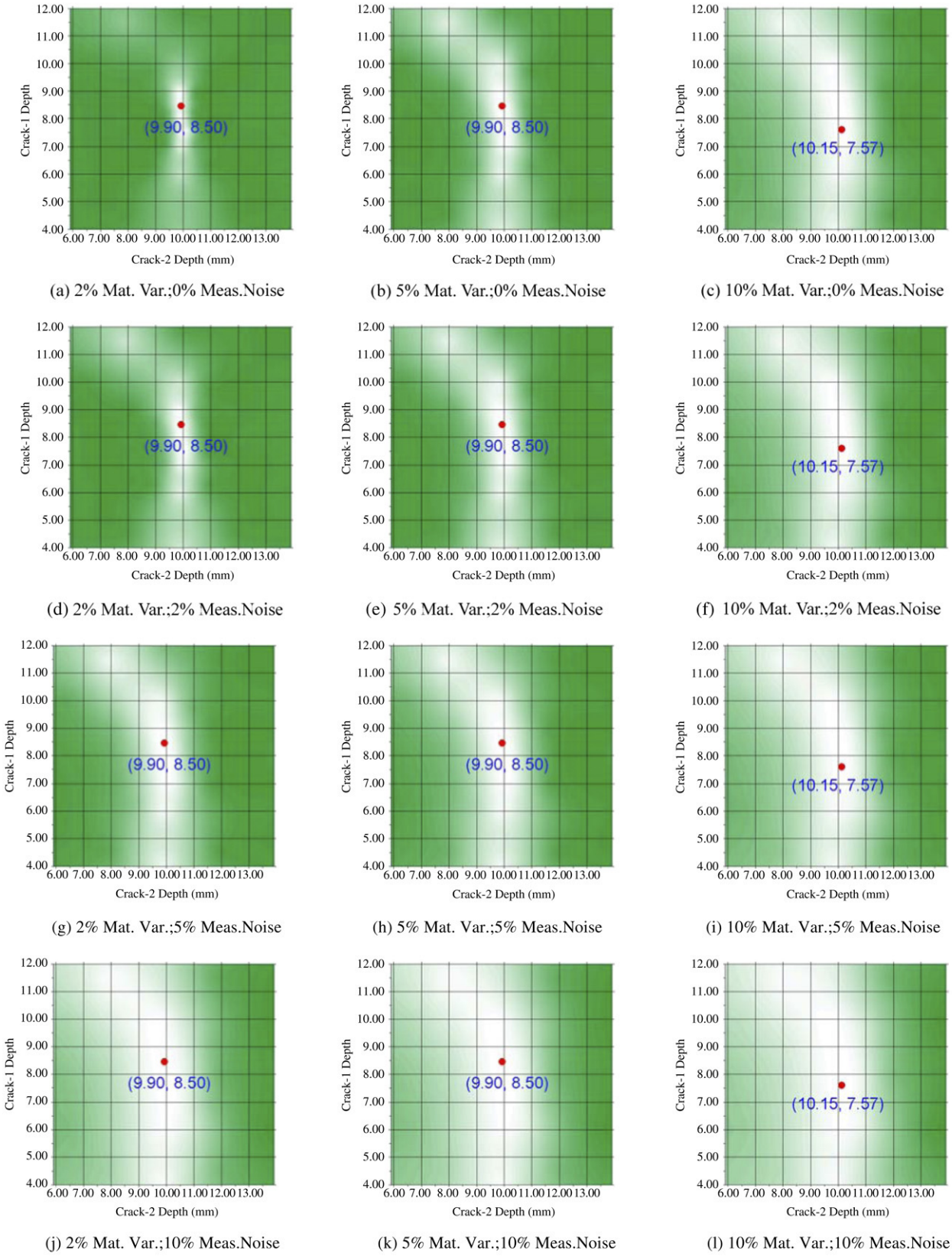

(a) 2% Mat. Var.;0% Meas.Noise (b) 5% Mat. Var.;0% Meas.Noise (c) 10% Mat. Var.;0% Meas.Noise

(d) 2% Mat. Var.;2% Meas.Noise (e) 5% Mat. Var.;2% Meas.Noise (f) 10% Mat. Var.;2% Meas.Noise

(g) 2% Mat. Var.;5% Meas.Noise (h) 5% Mat. Var.;5% Meas.Noise (i) 10% Mat. Var.;5% Meas.Noise

(j) 2% Mat. Var.;10% Meas.Noise (k) 5% Mat. Var.;10% Meas.Noise (l) 10% Mat. Var.;10% Meas.Noise

Fig. 17. Probability distribution (mode 1, crk.-1 loc. 243 mm, dep. 8 mm, crk.-2 loc. 243 mm, dep. 10 mm; 1st, 2nd and 3rd column for material variation 2%, 5% and 10% respectively; 1st, 2nd, 3rd and 4th row for measurement noise 0%, 2%, 5% and 10% respectively).

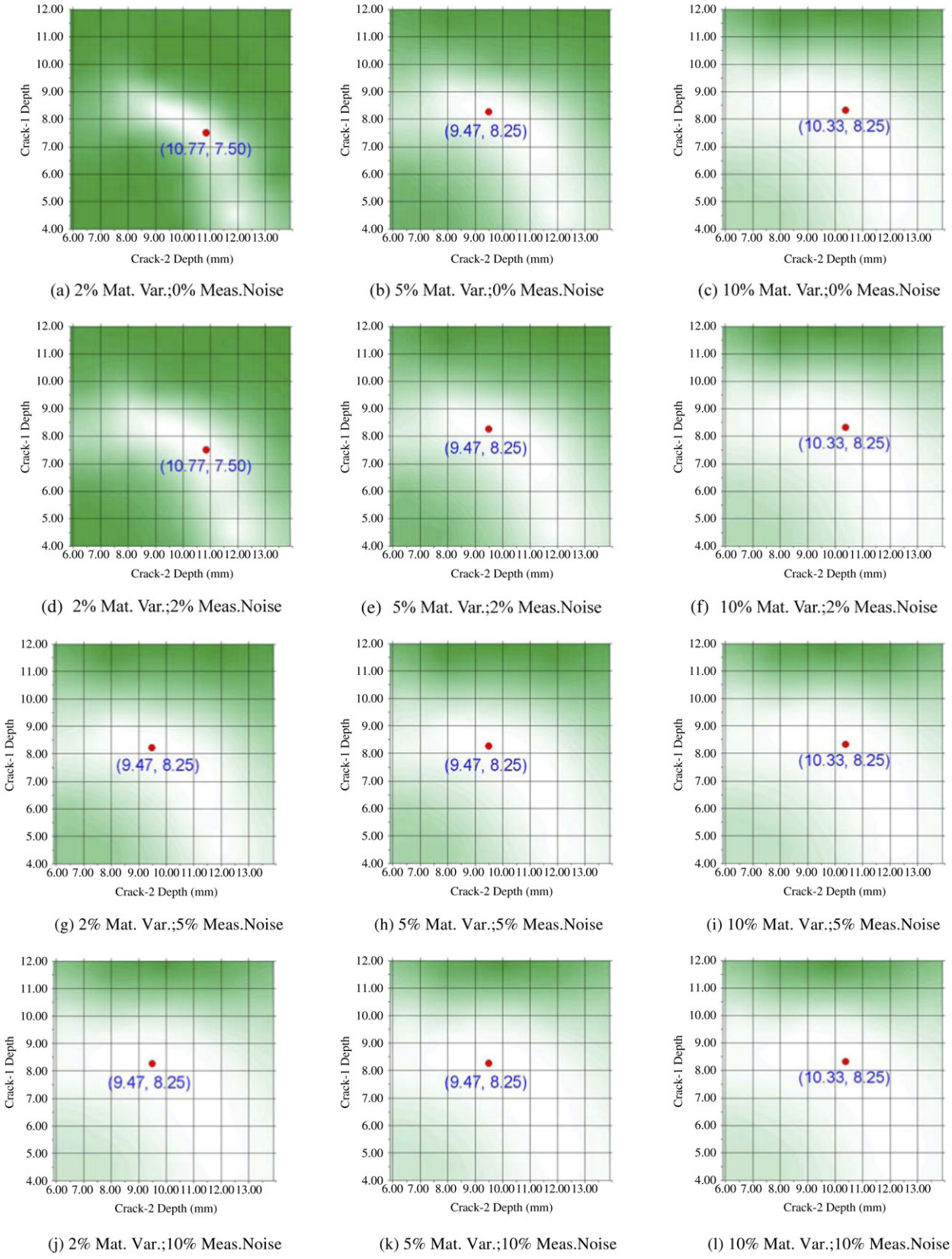

Fig. 18. Probability distribution (mode 2, crk.-1 loc. 243 mm, dep. 8 mm, crk.-2 loc. 243 mm, dep. 10 mm; 1st, 2nd and 3rd column for material variation 2%, 5% and 10% respectively; 1st, 2nd, 3rd and 4th row for measurement noise 0%, 2%, 5% and 10% respectively).

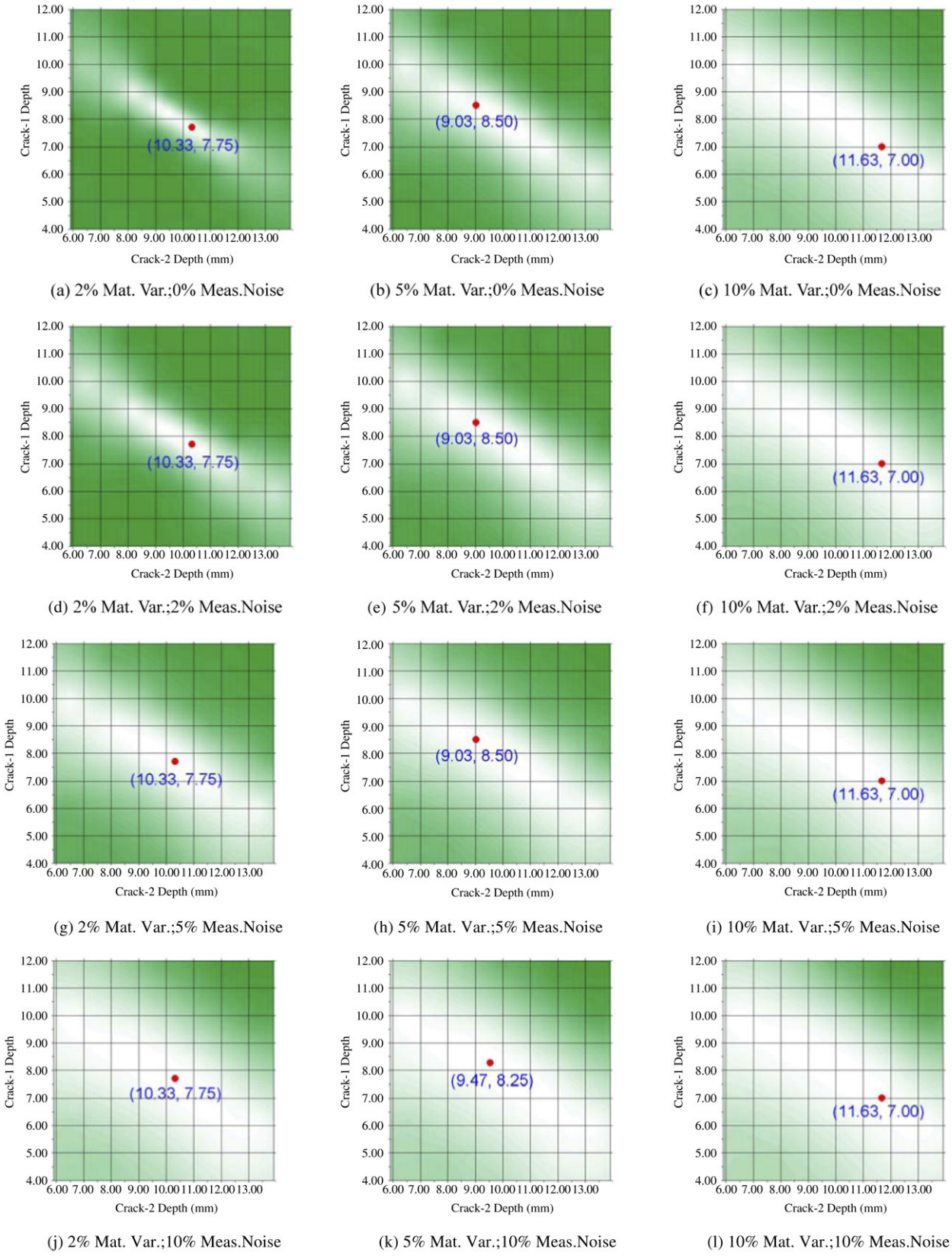

Fig. 19. Probability distribution (mode 3, crk.-1 loc. 243 mm, dep. 8 mm, crk.-2 loc. 243 mm, dep. 10 mm; 1st, 2nd and 3rd column for material variation 2%, 5% and 10% respectively; 1st, 2nd, 3rd and 4th row for measurement noise 0%, 2%, 5% and 10% respectively).

Table 3
Peak probability among material variation with different level measurement noise

Mode no.	EMA measure noise	Material variation (Mass density & Young's modulus)								
		$\sigma = \pm 2\%\mu$			$\sigma = \pm 5\%\mu$			$\sigma = \pm 10\%\mu$		
		Depth (mm)		Avg. err. of 2-crks (%)	Depth (mm)		Avg. err. of 2-crks (%)	Depth (mm)		Avg. err. of 2-crks (%)
		Crk-1	Crk-2		Crk-1	Crk-2		Crk-1	Crk-2	
1	$0\%\mu$	8.50	9.90	3.63	8.50	9.90	3.63	7.57	10.15	3.44
	$\pm 2\%\mu$	8.50	9.90	3.63	8.50	9.90	3.63	7.57	10.15	3.44
	$\pm 5\%\mu$	8.50	9.90	3.63	8.50	9.90	3.63	7.57	10.15	3.44
	$\pm 10\%\mu$	8.50	9.90	3.63	8.50	9.90	3.63	7.57	10.15	3.44
2	$0\%\mu$	7.50	10.77	6.98	8.25	9.47	4.21	8.25	10.33	3.21
	$\pm 2\%\mu$	7.50	10.77	6.98	8.25	9.47	4.21	8.25	10.33	3.21
	$\pm 5\%\mu$	8.25	9.47	4.21	8.25	9.47	4.21	8.25	10.33	3.21
	$\pm 10\%\mu$	8.25	9.47	4.21	8.25	9.47	4.21	8.25	10.33	3.21
3	$0\%\mu$	7.75	10.33	3.21	8.50	9.03	7.98	7.00	11.63	14.40
	$\pm 2\%\mu$	7.75	10.33	3.21	8.50	9.03	7.98	7.00	11.63	14.40
	$\pm 5\%\mu$	7.75	10.33	3.21	8.50	9.03	7.98	7.00	11.63	14.40
	$\pm 10\%\mu$	7.75	10.33	3.21	8.25	9.47	4.21	7.00	11.63	14.40

(6) The LDI works well for the location detection of the multiple-crack example (Beam-M case). We have the averaged absolute error 1.94% based on 18 impact location measurements. The FCI and statistical FCI database works well too: we have the averaged absolute error 0.50% for the invariant system and about 3.28% error for a system with material variation, and measurement noise less than 10%.
(7) For an unknown damage system with property-variant and noised frequency measurements, we should apply the lower mode for crack depth assessment to achieve a better solution. By applying the lower modal data, we should have the higher probability and confirmation in the severity identification.
(8) The pre-set resolution of FCI and statistical FCI database will affect the accuracy of depth identification. In the research, for the single-crack case the resolution ranged from 2.5% to 6.7% in beam depth, and from 0.30% to 2.5% for the multiple-crack case; it should be adjusted appropriately by specific requirements or by the engineering practice.
(9) In the paper, the authors have modeled the beams in free–free boundary conditions. Further studies are required for structure members in systems that are not in the same boundary condition.

References

[1] Allemang RJ, Brown DL. A correlation coefficient for modal vector analysis. In: Proceeding of 1st international modal analysis conference. 1983. p. 110–6.
[2] Barsoum RS. A degenerate solid element for linear fracture analysis of plate bending and general shells. International Journal of Numerical Method in Engineering 1976;10:551–64.
[3] Cawley P, Adams RD. The location of defects in structures from measurements of natural frequencies. Journal of Strain Analysis 1979; 14(2):49–57.
[4] Cornwell P, Farrar CR, Doebling SW, Sohn H. Environmental variability of modal properties. Experimental Techniques 1999;23(6):45–8.
[5] Doebling SW, Farrar CR, Prime MB, Shevitz DW. Damage identification and health monitoring of structural and mechanical systems from changes in their vibration characteristics: A literature review. Los Alamos national laboratory report, LA-13070-MS. 1996.
[6] Doebling SW, Farrar CF. Statistical damage identification techniques applied to the I-40 bridge over the Rio Grande River. In: Proceeding of 16th international modal analysis conference. 1998. p. 1717–24.
[7] Efron B, Tibshirani R. An introduction to the bootstrap in applied monographs on statistics and applied probability, vol. 57. Chapman and Hall; 1993.
[8] Freund J. Mathematical statistics. 5th ed. Englewood Cliffs (NJ): Prentice Hall; 1992. p. 462.
[9] Furukawa A, Otsuka H. Structural damage detection method using uncertain frequency response functions. Computer-Aided Civil and Infrastructure Engineering 2006;21:292–305.
[10] Ko JM, Wang JY, Ni YQ, Chak KK. Observation on environmental variability of modal properties of a cable-stayed bridge from one-year monitoring data. In: Chang F-K, editor. Structural health monitoring 2003 (Proc. 4th IWSHM). Lancaster: DEStech; 2003. p. 467–74.
[11] Mckay MD, Beckman RJ, Conover WJ. A comparison of three methods for selecting values of input variables in the analysis of output from a computer code. Technometrics 1979;21(2):239–45.
[12] Olsson A, Sanberg G, Dahlblom O. On the latin hypercube sampling for structural reliability analysis. Structure Safety 2003;25:47–68.
[13] Pandey AK, Biswas M, Samman MM. Damage detection from changes in curvature mode shape. Journal of Sound and Vibration 1991;145(2): 321–32.
[14] Peeters B, Roeck GD. One-year monitoring of the Z24-Bridge: Environmental effects versus damage events. Earthquake Engineering and Structural Dynamics 2001;30:149–71.
[15] Press WH, Teukolsky SA, Vetterling WT, Flannery BP. Numerical recipes in fortran. 2nd ed. Cambridge University Press; 1992. Section 15.6.
[16] Sikorsky C, Stubbs N, Guan F. The impact of natural frequency variation on damage detection. In: Chang F-K, editor. Structural health monitoring 2003 (Proc. 4th IWSHM). Lancaster: DEStech; 2003. p. 701–8.
[17] Sohn H, Dzwonczyk M, Straser EG, Kiremidjian AS, Law KH, Meng T. An experimental study of temperature effect on modal parameters of the Alamosa Canyon bridge. Earthquake Engineering and Structural Dynamics 1999;28(8):879–97.

[18] Sohn H, Farrar CR, Hemez FM, Shunk DD, Stinemates DW, Nadler BR. A review of structural health monitoring literature: 1996–2001. Los Alamos national laboratory report, LA-13976-MS. 2003.
[19] Stein M. Large sample properties of simulations using latin hypercube sampling. Technometrics 1987;29(2):143–51.
[20] Xia Y, Hao H. Statistical damage identification of structures with frequency changes. Journal of Sound and Vibration 2003;263(2):853–70.
[21] Xia Y, Hao H, Zanardo G, Deeks A. Long term vibration monitoring of an RC slab-temperature and humidity effect. Engineering Structures 2006; 28:441–52.
[22] Zienkiewicz OC. The finite element method: vol. II. 4th ed. Singapore: McGraw-Hill Book Co; 1989. p. 159–167.